Original Article

Institution of MECHANICAL ENGINEERS
Journal of AEROSPACE ENGINEERING

Proc IMechE Part G:
J Aerospace Engineering
0(0) 1–14

DOI: 10.1177/0954410013514346
uk.sagepub.com/jaero
SAGE

Periodic projectile linear theory for aerodynamically asymmetric projectiles

John Dykes[1], Mark Costello[2], Frank Fresconi[3] and Gene Cooper[3]

Abstract

A new analytical tool is proposed to aid in the design and performance evaluation of advanced guided projectile concepts. A projectile linear theory applicable to aerodynamically asymmetric configurations is created, leading to a linear, periodic dynamic system. Utilizing concepts in Floquet theory, stability of asymmetric projectile configurations is explored. While stability of many asymmetric projectile configurations can be accurately predicted using averaged linear, constant coefficient system dynamics, there are some configurations where the use of linear periodic systems theory is required for accurate stability prediction. This fact is shown by comparing stability boundaries of an example projectile configuration using the conventional projectile linear theory model and the new periodic projectile linear theory model.

Keywords

Asymmetric projectiles, Floquet theory, stability, flight dynamics

Date received: 24 March 2013; accepted: 29 October 2013

Introduction

Gun-launched guided munitions offer the ability to accurately track a desired 3D trajectory path, including impacting a desired point. In general, the gun-launch environment is a difficult one, presenting unique challenges such as extreme structural loads at launch, large projectile spin rates, and high cadence of fire. Upon being launched, munitions are then guided by control mechanisms to achieve a desired trajectory and impact a specific target. Over the past three decades, canards and fins have been employed extensively for trajectory control of projectiles. Popular examples include the U.S. Army's Copperhead[1,2] and Excalibur[3] development programs. Control mechanisms and onboard electronics suites for these types of munitions must be small due to size limitations and rugged to withstand extreme acceleration loads and high spin rates. Furthermore, since guided projectiles are often fired in large quantities, they must be relatively inexpensive to produce in order to be competitive. To meet these needs, numerous smart projectile concepts have been developed with aerodynamic asymmetries caused by the arrangement of lifting surfaces on the projectile body.[4–8]

Projectile linear theory (PLT) was developed in 1919 by Fowler et al.[9] and has since been an analytical workhorse in the ballistics community for the design and evaluation of nearly symmetric projectiles.[10] By linearizing the flight dynamic equations of motion through a series of simplifications and assumptions, classic PLT theory allows the engineer to quantify projectile performance using concepts from linear systems theory,[11,12] which are well understood and easily implemented. Due to the development of PLT theory, common tools at the ballisticians disposal include stability analysis, aerodynamic coefficient estimation using range data, and fast trajectory prediction.[13] Over time, classic PLT theory has been extended by various authors to handle more sophisticated aerodynamic models,[14] asymmetric mass properties,[15] fluid payloads,[16,17] moving internal parts,[13,18,19] dual-spin projectiles,[20,21] ascending flight,[22] lateral

[1]School of Aerospace Engineering, Georgia Institute of Technology, Atlanta, GA, USA
[2]School of Aerospace Engineering, School of Mechanical Engineering, Georgia Institute of Technology, Atlanta, GA, USA
[3]Weapons and Materials Research Directorate, U.S. Army Research Laboratories, Aberdeen, MD, USA

Corresponding author:
Mark Costello, Georgia Institute of Technology, Atlanta, GA 30332, United States.
Email: mark.costello@ae.gatech.edu

force impulses,[23–25] and model predictive control.[26] Recently, an extended linear theory for aerodynamically asymmetric lifting surfaces has been developed for a specific canard configuration to investigate the effects of canard dithering[27] and canard stall on projectile roll and pitch damping.[28]

The work reported here further extends PLT theory to account for general lifting surface configurations on a projectile body, including aerodynamically asymmetric configurations. Determination of stability bounds for these asymmetric configurations often requires the use of Floquet theory[29] to conduct stability analyses on linear time-periodic (LTP) systems. Using a current smart projectile concept as a motivating example, stability bounds are determined by LTP analysis and compared to the traditional linear time-invariant (LTI) analysis, which is shown to be inferior and inaccurate.

Nonlinear flight dynamic model

Equations of motion

The nonlinear flight dynamic model is a standard six-degree-of-freedom (6DOF) model. These ordinary differential equations are widely used in computational simulation of free flight vehicles and are reported in many sources including McCoy,[10] Etkin,[11] Carlucci,[30] and Murphy.[31] Derived using the standard Newton-Euler approach, these 12 equations of motion are provided in vector forms below, where the standard shorthand notation for trigonometric functions is used: $s_\alpha \equiv \sin(\alpha)$, $c_\alpha \equiv \cos(\alpha)$, and $t_\alpha \equiv \tan(\alpha)$.

$$\begin{Bmatrix} \dot{x} \\ \dot{y} \\ \dot{z} \end{Bmatrix} = \begin{bmatrix} c_\theta c_\psi & s_\phi s_\theta c_\psi - c_\phi s_\psi & c_\phi s_\theta c_\psi + s_\phi s_\psi \\ c_\theta s_\psi & s_\phi s_\theta s_\psi + c_\phi c_\psi & c_\phi s_\theta s_\psi - s_\phi c_\psi \\ -s_\theta & -s_\phi c_\theta & c_\phi c_\theta \end{bmatrix} \begin{Bmatrix} u \\ v \\ w \end{Bmatrix} \tag{1}$$

$$\begin{Bmatrix} \dot{\phi} \\ \dot{\theta} \\ \dot{\psi} \end{Bmatrix} = \begin{bmatrix} 1 & s_\phi t_\theta & c_\phi t_\theta \\ 0 & c_\phi & -s_\phi \\ 0 & s_\phi / c_\theta & c_\phi / c_\theta \end{bmatrix} \begin{Bmatrix} p \\ q \\ r \end{Bmatrix} \tag{2}$$

$$\begin{Bmatrix} \dot{u} \\ \dot{v} \\ \dot{w} \end{Bmatrix} = \begin{Bmatrix} X/m \\ Y/m \\ Z/m \end{Bmatrix} - \begin{bmatrix} 0 & -r & q \\ r & 0 & -p \\ -q & p & 0 \end{bmatrix} \begin{Bmatrix} u \\ v \\ w \end{Bmatrix} \tag{3}$$

$$\begin{Bmatrix} \dot{p} \\ \dot{q} \\ \dot{r} \end{Bmatrix} = [\mathbf{I}]^{-1} \left[\begin{Bmatrix} L \\ M \\ N \end{Bmatrix} - \begin{bmatrix} 0 & -r & q \\ r & 0 & -p \\ -q & p & 0 \end{bmatrix} [\mathbf{I}] \begin{Bmatrix} p \\ q \\ r \end{Bmatrix} \right] \tag{4}$$

The externally applied force vector in equation (3) is expressed in the body reference frame and decomposed into contributions due to weight, body aerodynamics, and lifting surface aerodynamics (X_C, Y_C, Z_C).

$$\begin{Bmatrix} X \\ Y \\ Z \end{Bmatrix} = W \begin{Bmatrix} -s_\theta \\ s_\phi c_\theta \\ c_\phi c_\theta \end{Bmatrix} - \frac{\pi}{8} \rho V^2 D^2 \begin{Bmatrix} C_{X0} + C_{X2}\left(v^2 + w^2\right)/V^2 \\ C_{NA} \frac{v}{V} - \frac{pD}{2V} C_{NPA} \frac{w}{V} \\ C_{NA} \frac{w}{V} + \frac{pD}{2V} C_{NPA} \frac{v}{V} \end{Bmatrix} + \begin{Bmatrix} X_C \\ Y_C \\ Z_C \end{Bmatrix} \tag{5}$$

The body aerodynamic loads in equation (5) can further be split into a steady air load contribution, which acts at the center of pressure, and a Magnus air load contribution, which acts at the center of Magnus force. The terms containing C_{NPA} constitute the Magnus air loads component, while the terms containing C_{X0}, C_{X2}, and C_{NA} define the loads acting at the center of pressure. The externally applied moment vector in equation (4) acts about the projectile mass center and in similar fashion can be decomposed into contributions from body aerodynamics and lifting surface aerodynamics (L_C, M_C, N_C).

$$\begin{Bmatrix} L \\ M \\ N \end{Bmatrix} = \frac{\pi}{8} \rho V^2 D^3 \begin{Bmatrix} C_{LDD} + \frac{pD}{2V} C_{LP} \\ C_{MA} \frac{w}{V} + \frac{qD}{2V} C_{MQ} + \frac{pD}{2V} C_{MPA} \frac{v}{V} \\ -C_{MA} \frac{v}{V} + \frac{rD}{2V} C_{MQ} + \frac{pD}{2V} C_{MPA} \frac{w}{V} \end{Bmatrix} + \begin{Bmatrix} L_C \\ M_C \\ N_C \end{Bmatrix} \tag{6}$$

The body aerodynamic loads in equation (6) act about the projectile mass center and can further be split into steady and unsteady air load contributions, as well as a Magnus air load contribution. The terms containing C_{LDD}, C_{LP}, and C_{MQ} constitute the unsteady air moments, while the terms containing C_{MA} and C_{MPA} constitute the steady and Magnus air moments, respectively. The moment contributions of the steady and Magnus air loads account for the effects of the center of pressure and center of Magnus force, which are in general not located at the mass center. For finned projectiles and other slow rolling airframes, the Magnus force contribution is usually negligible but is included here for model completeness and generality.

Lifting surface aerodynamic model

The lifting surface aerodynamic model implemented here is from Costello and Anderson,[32] which treats canard aerodynamic effects as a point force acting at the lifting surface aerodynamic center. An illustration of this model can be seen in Figure 1. The moment generated by this point force can then be computed

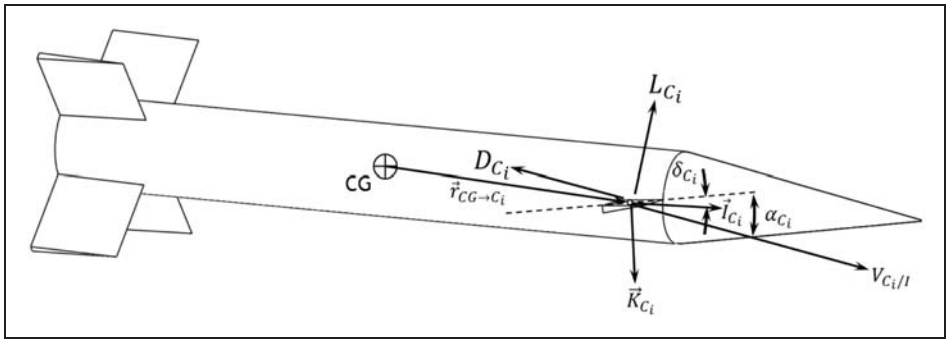

Figure 1. An illustration of a lifting surface aerodynamic model force diagram for an arbitrarily positioned canard-type lifting surface.

via cross product between the distance vector from the projectile mass center to the canard forces application point and the canard force.

By superposition, this model can account for an arbitrary number of lifting surfaces, positioned and oriented anywhere on a given parent projectile body.

$$\begin{Bmatrix} X_C \\ Y_C \\ Z_C \end{Bmatrix} = \sum_{i=1}^{n} \begin{Bmatrix} X_{C_i} \\ Y_{C_i} \\ Z_{C_i} \end{Bmatrix} \tag{7}$$

$$\begin{Bmatrix} L_C \\ M_C \\ N_C \end{Bmatrix} = \sum_{i=1}^{n} \begin{bmatrix} 0 & -\Delta WL_{C_i} & \Delta BL_{C_i} \\ \Delta WL_{C_i} & 0 & -\Delta SL_{C_i} \\ -\Delta BL_{C_i} & \Delta SL_{C_i} & 0 \end{bmatrix} \cdot \begin{Bmatrix} X_{C_i} \\ Y_{C_i} \\ Z_{C_i} \end{Bmatrix} \tag{8}$$

The expression for the point-force vector of the ith lifting surface in the projectile reference frame B is given below, where lifting surface aerodynamic lift and drag forces are determined in the ith lifting surface reference frame C_i.

$$\begin{Bmatrix} X_{C_i} \\ Y_{C_i} \\ Z_{C_i} \end{Bmatrix} = \frac{1}{2}\rho V^2 S_{C_i} \left[\mathbf{T}_{B\leftarrow C_i}\right] \cdot \begin{Bmatrix} C_{L_{C_i}} \sin\left(\alpha_{C_i} - \delta_{C_i}\right) - C_{D_{C_i}} \cos\left(\alpha_{C_i} - \delta_{C_i}\right) \\ 0 \\ -C_{L_{C_i}} \cos\left(\alpha_{C_i} - \delta_{C_i}\right) - C_{D_{C_i}} \sin\left(\alpha_{C_i} - \delta_{C_i}\right) \end{Bmatrix} \tag{9}$$

The single-axis transformation matrix used to move from the frame C_i back to frame B is shown in equation (10) by an azimuth angle defined in the projectile body roll plane.

$$\left[\mathbf{T}_{B\leftarrow C_i}\right] = \begin{bmatrix} 1 & 0 & 0 \\ 0 & c_{\phi_{C_i}} & -s_{\phi_{C_i}} \\ 0 & s_{\phi_{C_i}} & c_{\phi_{C_i}} \end{bmatrix} \tag{10}$$

The aerodynamic angle of attack for the ith lifting surface in equation (11) is a function of local air velocity components, which can be expressed as a function of body-frame states according to the two-point-fixed-on-a-rigid-body formula.

$$\alpha_{C_i} = \tan^{-1}\left(\frac{w_{C_i}}{u_{C_i}}\right) + \delta_{C_i} \tag{11}$$

Linear flight dynamic model

The 6DOF rigid body projectile model discussed above consists of 12 highly nonlinear differential equations for which a closed-form solution has not been directly found. Significant work has been performed to simplify the equations of motion such that an accurate analytical solution can be determined and is discussed in detail by McCoy[10] and Ollerenshaw and Costello.[26] Linearizing assumptions include: (1) small-angle approximations for aerodynamic angles of attack and the Euler yaw angle; (2) the projectile is mass-balanced such that (i) the mass center lies in the rotational axis of symmetry and (ii) the inertia tensor reduces to a diagonal matrix of axial and transverse inertias; and (3) products of small quantities with each other (e.g., θ, ψ, $\tilde{v}$, $\tilde{w}$, $\tilde{q}$, and $\tilde{r}$) are negligible. Additionally, linearizing simplifications include: (1) a change of variables is made from the velocity along the projectile axis of symmetry u, to the total velocity V; (2) dimensionless arc length, s, is used as the independent variable instead of time t; and (3) rather than employing a reference frame fixed to the projectile body, PLT theory uses an intermediate reference frame, which is aligned with the projectile axis of symmetry but does not roll. Lateral translational and rotational velocity components described in this frame, known as the no-roll (NR) frame, are denoted with a '$\sim$' overscore.

Montalvo and Costello[28] proposed an extension of the classic PLT assumptions and simplifications to be applied to an arbitrary set of lifting surfaces, which can cause aerodynamic asymmetries on a projectile. The extended assumptions include: (1) the total velocities experienced by lifting surfaces are approximately equal to the projectile mass center total velocity; (2) the lifting surface angles of attack are

assumed small; and (3) the trigonometric functions $\sin(\alpha_{C_i} - \delta_{C_i})$ and $\cos(\alpha_{C_i} - \delta_{C_i})$ from equation (9) can be linearized by utilizing a velocity triangle diagram approach and small-angle approximation.

Applying the extended PLT theory assumptions to the lifting surface aerodynamic model, all six of the total lifting surface force/moment components ($\tilde{X}'_C$, $\tilde{Y}'_C$, $\tilde{Z}'_C$, $\tilde{L}'_C$, $\tilde{M}'_C$, and $\tilde{N}'_C$) become quasi-linear with total velocity V, roll rate p, and roll angle ϕ states still appearing nonlinearly within these expressions. To remedy this, a simplification is made to decompose all total velocity and roll rate expressions into linear components (V, p) and constant components (V_o, p_o). This simplification is valid if V and p change slowly with respect to time and other state variables. The nonlinearities due to roll angle ϕ are more complex and will be considered later in the discussion on flight dynamic stability. Equation (12) shows a general form for this reduction for the force component (divided by mass for consistency).

$$\begin{aligned}\frac{1}{m}\tilde{X}'_C = {} & \tilde{X}'_V \cdot V + \left(\tilde{X}'_p + \tilde{X}'_{pp}p_o\right) \cdot p \\ & + \left(\tilde{X}'_{\tilde{v}} + \tilde{X}'_{\tilde{v}p}p_o\right) \cdot \tilde{v} + \left(\tilde{X}'_{\tilde{w}} + \tilde{X}'_{\tilde{w}p}p_o\right) \cdot \tilde{w} \\ & + \left(\tilde{X}'_{\tilde{q}} + \tilde{X}'_{\tilde{q}p}p_o\right) \cdot \tilde{q} + \left(\tilde{X}'_{\tilde{r}} + \tilde{X}'_{\tilde{r}p}p_o\right) \cdot \tilde{r}\end{aligned} \tag{12}$$

From the above expression, the coefficients $\tilde{X}'_V$, $\tilde{X}'_p$, $\tilde{X}'_{pp}$, $\tilde{X}'_{\tilde{v}}$, $\tilde{X}'_{\tilde{v}p}$, $\tilde{X}'_{\tilde{w}}$, $\tilde{X}'_{\tilde{w}p}$, $\tilde{X}'_{\tilde{q}}$, $\tilde{X}'_{\tilde{q}p}$, $\tilde{X}'_{\tilde{r}}$, and $\tilde{X}'_{\tilde{r}p}$ are constant with respect to all state variables except ϕ. These coefficients are also functions of n number of lifting surface geometric parameters, which in general appear nonlinearly. For the ith lifting surface, these include: position components—ΔSL_{C_i}, ΔBL_{C_i}, and ΔWL_{C_i}; orientation angles—ϕ_{C_i} and δ_{C_i}; planform area—S_{C_i}; and aerodynamic data—$C_{L_{C_i}}$ and $C_{D_{C_i}}$. Refer to the Appendix 2 for a complete summary of these expressions. The effect of incorporating the lifting surface force/moment components into classic PLT theory acts to fully couple the dynamic equations of motion; however, the kinematic equations remain unchanged.

The derived extended PLT dynamic equations of motion can be posed as a nonhomogeneous linear system of ordinary differential equations, as shown in equation (13), which can be readily analyzed using standard techniques as shown by Kreyszig[33] and Miller and Michel.[29] The linearization condition for this system is defined through the values $(V_o, p_o, \phi_o, \theta_o)$, where θ_o only influences the gravitational forcing terms and treatment of ϕ_o will be addressed later in the discussion on flight dynamic stability

$$x' = \mathbf{A}x + \boldsymbol{B} \tag{13}$$

The state vector and state vector derivative with respect to arc length are defined as follows.

$$x = \left\{ V \quad p \quad \tilde{v} \quad \tilde{w} \quad \tilde{q} \quad \tilde{r} \right\}^T \tag{14}$$

$$x' = \left\{ V' \quad p' \quad \tilde{v}' \quad \tilde{w}' \quad \tilde{q}' \quad \tilde{r}' \right\}^T \tag{15}$$

The system homogeneous matrix $\mathbf{A}$ and nonhomogeneous forcing function vector $\boldsymbol{B}$ are defined as follows.

$$\mathbf{A} = t \begin{bmatrix} \tilde{X}'_V + C'_{VV} & \tilde{X}'_p + \tilde{X}'_{pp}p_o & \tilde{X}'_{\tilde{v}} + \tilde{X}'_{\tilde{v}p}p_o & \tilde{X}'_{\tilde{w}} + \tilde{X}'_{\tilde{w}p}p_o & \tilde{X}'_{\tilde{q}} + \tilde{X}'_{\tilde{q}p}p_o & \tilde{X}'_{\tilde{r}} + \tilde{X}'_{\tilde{r}p}p_o \\ \tilde{L}'_V + C'_{pV} & \tilde{L}'_p + \tilde{L}'_{pp}p_o + C'_{pp} & \tilde{L}'_{\tilde{v}} + \tilde{L}'_{\tilde{v}p}p_o & \tilde{L}'_{\tilde{w}} + \tilde{L}'_{\tilde{w}p}p_o & \tilde{L}'_{\tilde{q}} + \tilde{L}'_{\tilde{q}p}p_o & \tilde{L}'_{\tilde{r}} + \tilde{L}'_{\tilde{r}p}p_o \\ \tilde{Y}'_V & \tilde{Y}'_p + \tilde{Y}'_{pp}p_o & \tilde{Y}'_{\tilde{v}} + \tilde{Y}'_{\tilde{v}p}p_o + C'_{\tilde{v}\tilde{v}} & \tilde{Y}'_{\tilde{w}} + \tilde{Y}'_{\tilde{w}p}p_o & \tilde{Y}'_{\tilde{q}} + \tilde{Y}'_{\tilde{q}p}p_o & \tilde{Y}'_{\tilde{r}} + \tilde{Y}'_{\tilde{r}p}p_o + C'_{\tilde{v}\tilde{r}} \\ \tilde{Z}'_V & \tilde{Z}'_p + \tilde{Z}'_{pp}p_o & \tilde{Z}'_{\tilde{v}} + \tilde{Z}'_{\tilde{v}p}p_o & \tilde{Z}'_{\tilde{w}} + \tilde{Z}'_{\tilde{w}p}p_o + C'_{\tilde{w}\tilde{w}} & \tilde{Z}'_{\tilde{q}} + \tilde{Z}'_{\tilde{q}p}p_o + C'_{\tilde{w}\tilde{q}} & \tilde{Z}'_{\tilde{r}} + \tilde{Z}'_{\tilde{r}p}p_o \\ \tilde{M}'_V & \tilde{M}'_p + \tilde{M}'_{pp}p_o & \tilde{M}'_{\tilde{v}} + \tilde{M}'_{\tilde{v}p}p_o + C'_{\tilde{q}\tilde{v}} & \tilde{M}'_{\tilde{w}} + \tilde{M}'_{\tilde{w}p} + C'_{\tilde{q}\tilde{w}} & \tilde{M}'_{\tilde{q}} + \tilde{M}'_{\tilde{q}p}p_o + C'_{\tilde{q}\tilde{q}} & \tilde{M}'_{\tilde{r}} + \tilde{M}'_{\tilde{r}p}p_o + C'_{\tilde{q}\tilde{r}} \\ \tilde{N}'_V & \tilde{N}'_p + \tilde{N}'_{pp}p_o & \tilde{N}'_{\tilde{v}} + \tilde{N}'_{\tilde{v}p}p_o + C'_{\tilde{r}\tilde{v}} & \tilde{N}'_{\tilde{w}} + \tilde{N}'_{\tilde{w}p} + C'_{\tilde{r}\tilde{w}} & \tilde{N}'_{\tilde{q}} + \tilde{N}'_{\tilde{q}p}p_o + C'_{\tilde{r}\tilde{q}} & \tilde{N}'_{\tilde{r}} + \tilde{N}'_{\tilde{r}p}p_o + C'_{\tilde{r}\tilde{r}} \end{bmatrix} \tag{16}$$

$$\boldsymbol{B} = \left\{ G'_V \quad 0 \quad 0 \quad G'_{\tilde{w}} \quad 0 \quad 0 \right\}^T \tag{17}$$

From the above expressions, the coefficients C'_{VV}, C'_{pV}, C'_{pp}, $C'_{\tilde{v}\tilde{v}}$, $C'_{\tilde{v}\tilde{r}}$, $C'_{\tilde{w}\tilde{w}}$, $C'_{\tilde{w}\tilde{q}}$, $C'_{\tilde{q}\tilde{v}}$, $C'_{\tilde{q}\tilde{w}}$, $C'_{\tilde{q}\tilde{q}}$, $C'_{\tilde{q}\tilde{r}}$, $C'_{\tilde{r}\tilde{v}}$, $C'_{\tilde{r}\tilde{w}}$, $C'_{\tilde{r}\tilde{q}}$, and $C'_{\tilde{r}\tilde{r}}$, are the inertial and symmetric body aerodynamic expressions derived in classic PLT theory, where G'_V and $G'_{\tilde{w}}$ are gravitational expressions. Refer to the Appendix 2 for a complete summary of these expressions.

The extended PLT coefficient matrix in equation (16) offers insight into the aerodynamic contributions of lifting surfaces during flight. The addition of asymmetric lifting surfaces fully couples all six dynamic

states. This differs from classic PLT theory where the total velocity and roll rate dynamics decouple from the other four epicyclic states ($\tilde{v}$, $\tilde{w}$, $\tilde{q}$, and $\tilde{r}$).

The aerodynamic effects of simple symmetric lifting surface configurations within the extended PLT theory can be significantly less complex due to canceling terms. In the case of symmetric four-finned projectiles, the extended PLT theory is analytically identical to the classic PLT theory and V and p are decoupled from the epicyclic dynamics. A closer look at the lifting surface coefficient expressions (see Appendix 2) reveals that the extended PLT theory is periodic in ϕ, since this state always appears within trigonometric functions of the plant matrix.

Stability theory

The extended PLT equations of motion represent a linear periodic dynamic system, and as such, stability must be evaluated using Floquet theory.[29] For small aerodynamic asymmetries, the periodic part of the dynamic matrix $\mathbf{A}$ and forcing function vector $\boldsymbol{B}$ is small and standard linear systems theory can be used to evaluate stability without a notable loss in accuracy. It should be noted that classic stability theory formulas for projectiles assume the underlying dynamic system is LTI, even for aerodynamically asymmetric configurations.

For an LTI system

$$\dot{x} = \mathbf{A}x + \boldsymbol{B}, \tag{18}$$

stability of the system is determined from the eigenvalues of the matrix $\mathbf{A}$ with conditions for a stable system being that the real part of all eigenvalues is less than zero. With this approach, $(V_o, p_o, \phi_o, \theta_o)$ are all chosen to be constant values for a specified operating condition.

For an LTP system

$$\dot{x} = \mathbf{A}(t)x + \boldsymbol{B}, \tag{19}$$

where the matrix $\mathbf{A}(t)$ is periodic with a period T equal to the time of a complete roll cycle.

$$T = \frac{2\pi}{p_o} \tag{20}$$

For the matrix above (equation (16)) to be periodic, it is assumed that the projectile is rolling at a near constant rate; therefore, treating the roll angle ϕ as a linear function of time.

$$\phi(t) = p_o t + \phi_o \tag{21}$$

The previous relationship effectively converts the periodic effects of roll angle into the time domain; however, care must be taken before evaluating an airframe where near constant roll rates are not observed. Now Floquet theory can be implemented on the linear periodic system due to the following important mathematical property.

$$\mathbf{A}(t) = \mathbf{A}(t + NT), \quad \text{for } N = 0 \pm 1, \pm 2, \ldots, \pm\infty \tag{22}$$

Equation (22) implies that if the independent variable t is replaced by $t + T$, the system dynamics of equation (13) remain invariant. Because of this, the fundamental matrix for the system of equation (19) can be expressed in a special form known as the *Floquet decomposition*:[12]

$$\Phi(t) = \mathbf{P}(t) \cdot e^{\mathbf{R}t} \cdot \mathbf{P}^{-1}(0), \tag{23}$$

where the continuous, invertible matrix $\mathbf{P}(t)$ contains the periodic information of $\mathbf{A}$ and the constant matrix $\mathbf{R}$ contains the characteristic information of $\mathbf{A}$. In general, Floquet decomposition can be performed for any linear system. For example, in the case of an LTI system, $\mathbf{P}(t)$ reduces to the identity matrix and $\mathbf{R} = \mathbf{A}$.

A principle result of Floquet theory is that the stability of equation (19) can be ascertained from the characteristic exponent matrix $\mathbf{R}$. To this end, equation (19) is evaluated at $t = T$ to yield the following expression.

$$\Phi(T) = \mathbf{P}(0) \cdot e^{\mathbf{R}T} \cdot \mathbf{P}^{-1}(0) \tag{24}$$

For the general nth order system, the matrix $e^{\mathbf{R}T}$ is called the characteristic multiplier matrix. Equation (24) is a similarity transformation; hence, the eigenvalues between $\Phi(T)$ and $e^{\mathbf{R}T}$ are preserved.

$$\mu_j = \text{eig}(\Phi(T)) = \text{eig}\left(e^{\mathbf{R}T}\right), \quad \text{for all } (1 < j < n) \tag{25}$$

The eigenvalues of $e^{\mathbf{R}T}$ are μ_j and can be related to η_j, the eigenvalues of $\mathbf{R}$, by the relation below.

$$\mu_j = e^{\eta_j T}, \quad \text{for all } (1 < j < n) \tag{26}$$

Thus, the eigenvalues of the characteristic exponent matrix $\mathbf{R}$ can be found through algebraic manipulation of equation (26). Because values of μ_i can be complex, the complex identity for the logarithm operator must be employed,[34] as is shown in equation (27).

$$\eta_j = \frac{1}{T}\log(\mu_j) = \frac{1}{T}\ln|\mu_j| + \frac{1}{T}\left(\arg(\mu_j) + 2\pi k\right)i, \quad \text{where } k = 0, \pm 1, \ldots, \pm\infty \tag{27}$$

Now by considering the real part of η_j, stability of the LTP system can be evaluated using the standard criteria. Note that the imaginary part of η_j is nonunique and other considerations are needed to determine the integer value k. For more details on Floquet theory, consult Miller and Michel.[29]

Results

Recently, an affordable precision munition concept was developed and demonstrated in guided flight experiments.[35] This concept was aerodynamically asymmetric, featuring a pair of canards on the nose and canted tail fins to roll the projectile in flight (see Figure 2). Because of the lack of an analytical approach to quantify the influence of periodic effects due to aerodynamic asymmetries, these airframes were not properly sized to maximize maneuverability while still ensuring flight dynamic stability. Using a testbed projectile with a similar canard configuration, periodic PLT will be used to properly characterize the flight dynamics and predict stability boundaries for varying flight conditions, canard sizes, and projectile mass center positioning.

The Army-Navy basic finner is used as a testbed projectile to mimic the canard configuration of the very affordable precision projectile (VAPP) airframe. Flight mechanics of this projectile are well understood and data are readily available. From Dupuis,[36] the projectile mass, length, diameter (D), mass center measured along the stationline ($SLCG$), roll inertia, and pitch inertia are 0.108851 slugs, 0.9842 ft, 0.098425 ft, 0.4429 ft, 0.000142 slugs-ft^2, and 0.00728 slugs-ft^2, respectively. The fins are equally sized with the chord and planform both measuring 0.098425 ft in length. For the nominal configuration shown in Figure 3, two canards are appended to the projectile

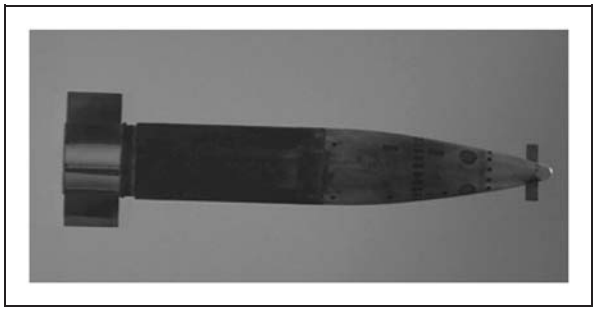

Figure 2. The very affordable precision projectile (VAPP) smart munitions concept currently being developed by the U.S. Army.

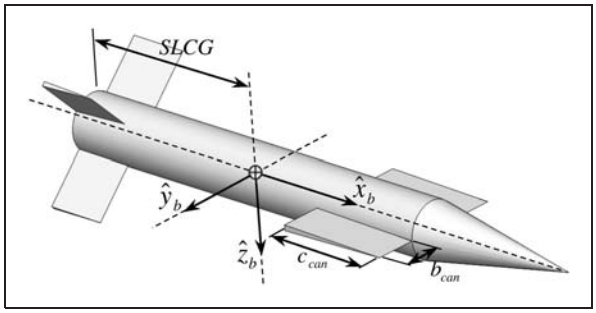

Figure 3. Illustration of the four-fin, two-canard baseline projectile configuration.
SLCG: projectile stationline center of gravity positioning

180° apart with half aspect ratio of the four fins but two times the planform area. The stationline positioning of each canard half-chord is located in the horizontal plane with a leading edge distance of 0.2795 ft from the nose of the projectile. All aerodynamic coefficients for the Army-Navy basic finner are estimated as a function of Mach number using standard aeroprediction techniques, e.g., the software package PRODAS.[37]

Flight dynamic simulation of an asymmetric projectile

Nonlinear 6DOF results obtained from an industry standard flight simulation software called BOOM[32] were used for comparison with extended LTI and LTP model trajectories. For the projectile airframe of Figure 3, correlation between LTP and nonlinear 6DOF trajectory results is good, while correlation between LTI and nonlinear 6DOF trajectory results degrade with increasing asymmetry (i.e., canard sizing). Furthermore, for the case where the mass center is located at $(SLCG/SLCG_{nom}) = 0.6$, the LTP model predicts a highly stable projectile; however, the LTI approximation predicts a marginally stable projectile. Figures 4–10 compare trajectory results between 6DOF, LTP, and LTI models, where $(SLCG/SLCG_{nom}) = 0.6$, $(b_{can}/D) = 0.4$, and $(c_{can}/D) = 2.0$. Nonzero initial conditions are $\theta = 1.6023°$, $V = 558.0$ ft/s (Mach 0.5), $p = 100$ rad/s. The four rear fins were canted to a value $\delta_{fin} = 0.475°$ to encourage a constant projectile roll rate throughout flight. These figures demonstrate the ability of the LTP model to approximate the 6DOF model when fin cant is used to encourage near constant roll rate through flight. Throughout 1.0 s of flight, error between LTP and 6DOF models is due

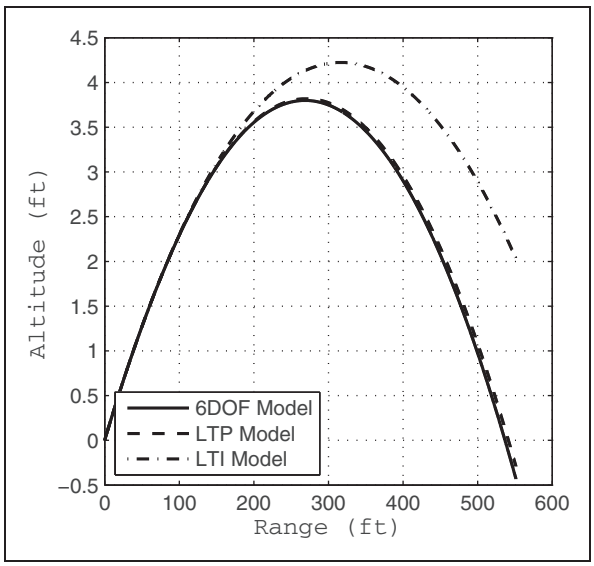

Figure 4. Altitude vs. range.
LTI: linear time-invariant; LTP: linear time-periodic; 6DOF: six-degree-of-freedom

to the assumption that total velocity and roll rate are slowly changing within the dynamic matrix **A** of the LTP model. Error between LTI and LTP models is due to the failure of the LTI model to account for periodic effects.

Effects of mass center positioning and flight speed on maximum allowable canard sizing

The stability analysis previously discussed can be used to calculate the maximum allowable canard sizing for variation in mass center positioning and flight speed. Also, the effects of different roll rates can be considered; however, canard surface sizing was observed to be insensitive to reasonable variations in roll rate for the given airframe of Figure 3. Additionally, because Floquet theory is capable of accounting for the periodic effects commonly observed in asymmetric projectiles, the limitation of LTI stability analysis can be quantified. To demonstrate this, consider the projectile of Figure 3, where the projectile mass center is varied from the nominal location between $0.4 \leqslant (SLCG/SLCG_{nom}) \leqslant 1.0$ from the projectile rear. LTP and LTI results were both determined for three flight speeds: Mach 0.5, 2.0, and 3.0. Transonic flight speeds were not considered here but easily could be if aerodynamic data were readily available.

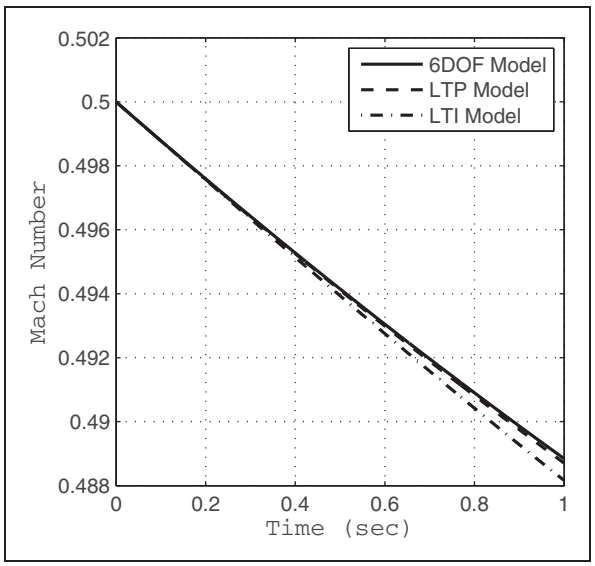

Figure 5. Mach number vs. time.
LTI: linear time-invariant; LTP: linear time-periodic; 6DOF: six-degree-of-freedom

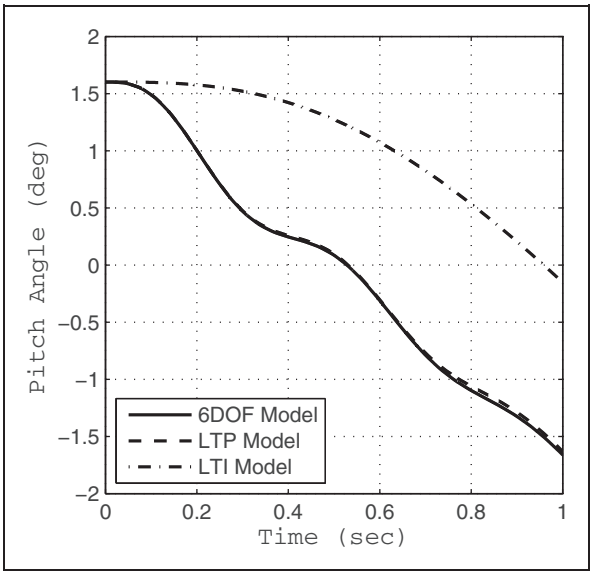

Figure 7. Pitch angle vs. time.
LTI: linear time-invariant; LTP: linear time-periodic; 6DOF: six-degree-of-freedom

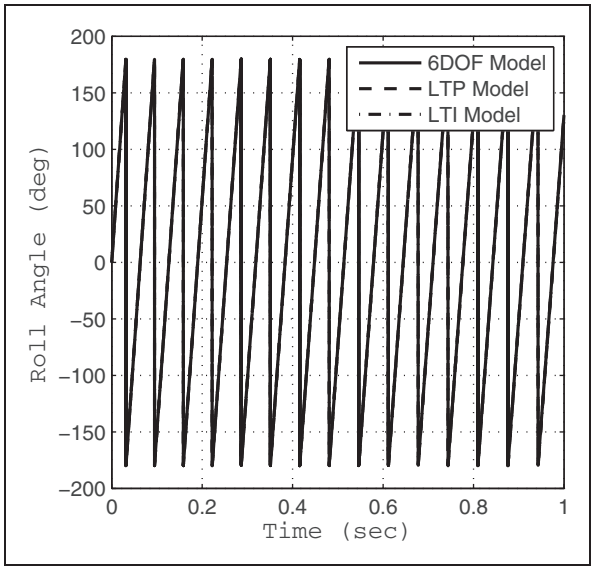

Figure 6. Roll angle vs. time.
LTI: linear time-invariant; LTP: linear time-periodic; 6DOF: six-degree-of-freedom

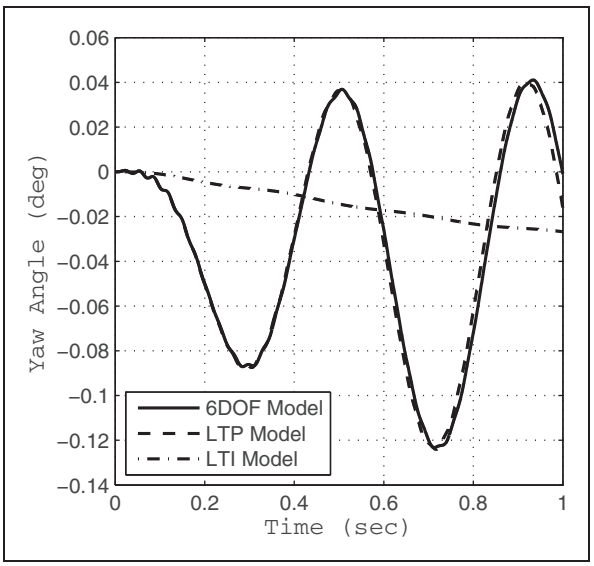

Figure 8. Yaw angle vs. time.
LTI: linear time-invariant; LTP: linear time-periodic; 6DOF: six-degree-of-freedom

The quasi-linear state p_o and ϕ_o were set to 100 rad/s and 0.0°, respectively.

Figure 11 shows the maximum allowable canard length, $(b_{can}/D)_{max}$, for stability versus stationline

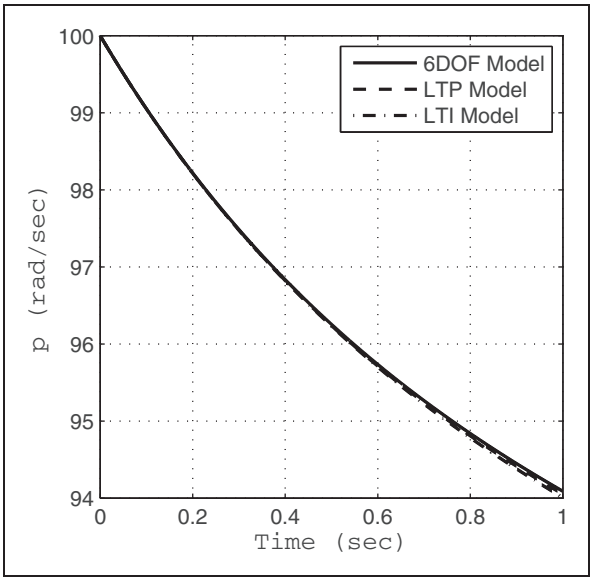

Figure 9. Roll rate vs. time.
LTI: linear time-invariant; LTP: linear time-periodic; 6DOF: six-degree-of-freedom

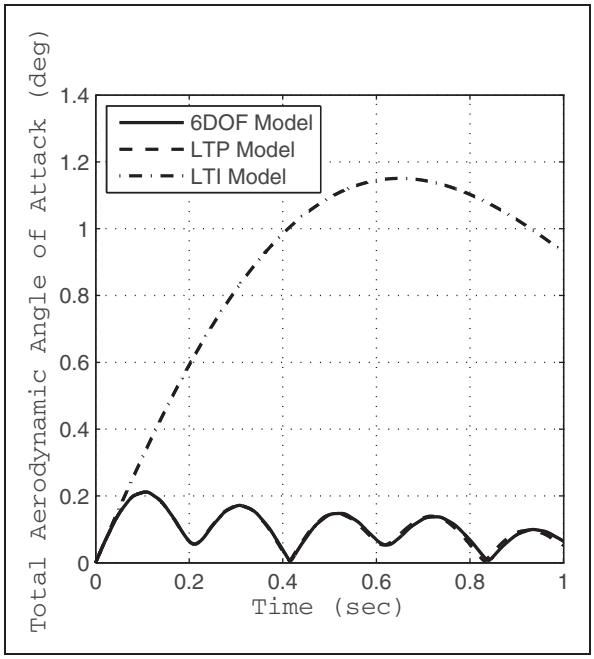

Figure 10. Total aerodynamic angle of attack vs. time.
LTI: linear time-invariant; LTP: linear time-periodic; 6DOF: six-degree-of-freedom

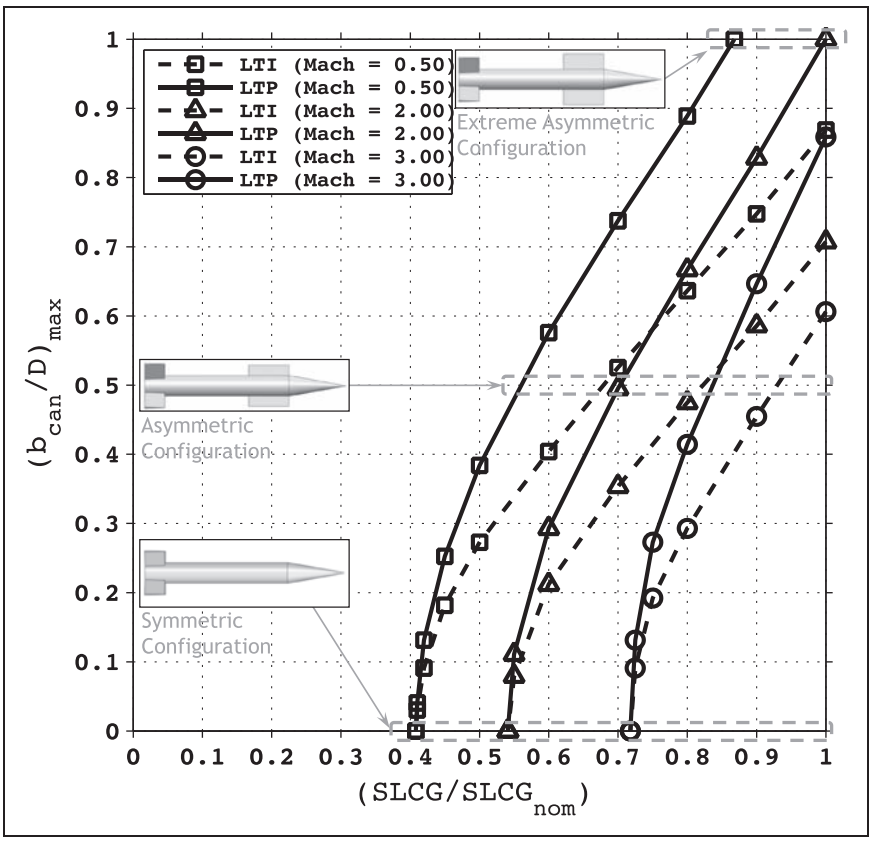

Figure 11. Stability map showing the maximum allowable canard surface sizing versus mass center positioning and flight speed.
LTI: linear time-invariant; LTP: linear time-periodic; SLCG: projectile stationline center of gravity positioning

mass center positioning at different flight speeds. LTP model predictions of $(b_{can}/D)_{max}$ are solid lines, while LTI model results are dashed lines. As can be seen, both models show similar trends. The first trend is that as $(SLCG/SLCG_{nom})$ is moved rearward, $(b_{can}/D)_{max}$ decreases. A second trend is that as Mach number increases, $(b_{can}/D)_{max}$ decreases. Finally, models converge upon each other for the cases where $(b_{can}/D)_{max} = 0$, and thus no periodic effects are present. For increasing $(SLCG/SLCG_{nom})$, the LTI model increasingly under-predicts $(b_{can}/D)_{max}$, and the difference between the LTP and LTI models for a given mass center positioning and Mach number represents the loss of available maneuverability predicted by the LTI model. These results are useful when maximizing maneuverability is a priority but mass center positioning is not yet defined within a design.

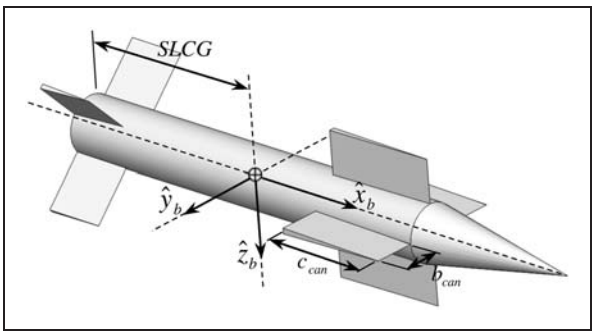

Figure 12. Illustration of the four-fin, four-canard baseline projectile configuration.
SLCG: projectile stationline center of gravity positioning

From Figure 11, it was observed that the LTP and LTI converge to identical results when $(b_{can}/D)_{max} = 0$, which corresponds to a symmetric projectile. As previously mentioned, LTI models using classical linear theory have been extensively employed to describe symmetric configurations. Consider the symmetric configuration of Figure 12, which is similar to the configuration of Figure 3 except that it has an axisymmetric four-canard configuration. As was previously done for the asymmetric case, a stability analysis was conducted to determine the maximum allowable canard sizing for variation in mass center positioning and flight speed. Again, the projectile mass center is varied from the nominal location between $0.4 \leqslant (SLCG/SLCG_{nom}) \leqslant 1.0$ from the projectile rear, and LTP and LTI results were both determined for three flight speeds: Mach 0.5, 2.0, and 3.0. The quasi-linear state p_o and ϕ_o were set to 100 rad/s and 0.0°, respectively.

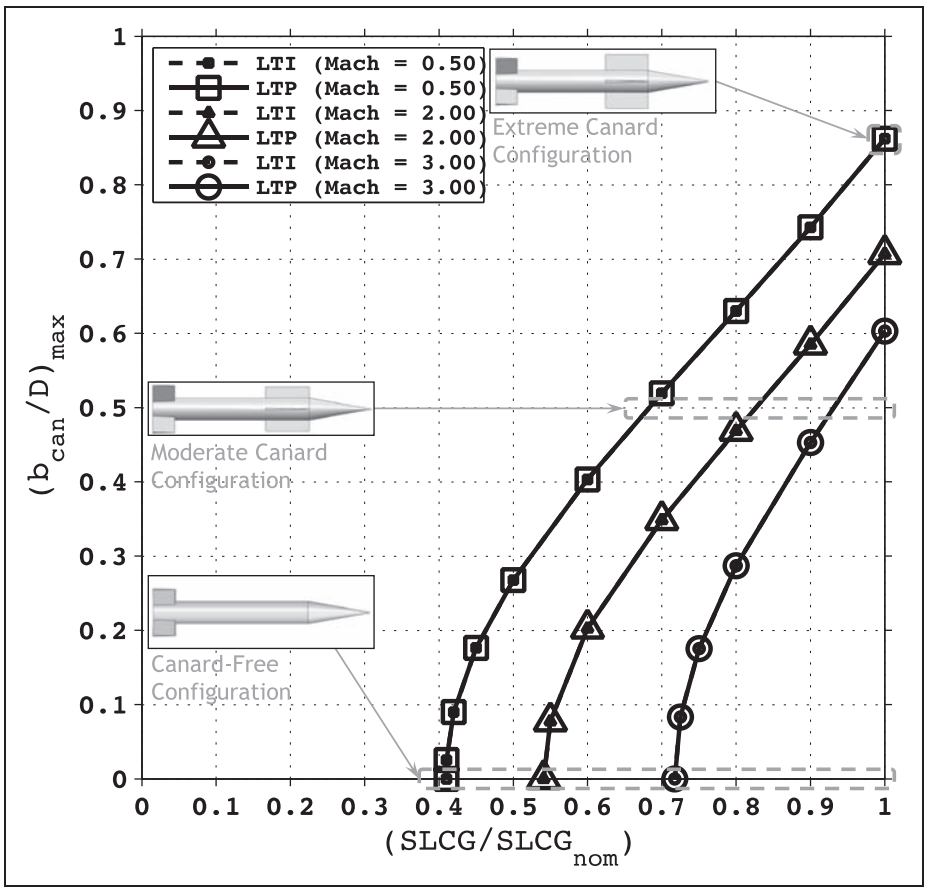

Figure 13. Stability map showing the maximum allowable canard surface sizing versus mass center positioning and flight speed.
LTI: linear time-invariant; LTP: linear time-periodic; 6DOF: six-degree-of-freedom

Figure 13 shows the maximum allowable canard length, $(b_{can}/D)_{max}$, for stability versus stationline mass center positioning at different flight speeds. It is observed that LTP and LTI predictions for each flight speed are identical for the case of a symmetric projectile. Thus in the case of a symmetric projectile, LTP models reduce to LTI approximations and Floquet stability theory predictions are identical to standard stability predictions for LTI systems.

Conclusions

Classic PLT was extended to account for aerodynamic effects of generally asymmetric lifting surfaces to provide the ballistician with a new analytical tool to help quantify asymmetric projectile performance. These added effects generally introduce periodic terms into the linear model of the projectile, and fully couple the linearized dynamic equations of motion. Conducting an LTI stability analysis on an asymmetric projectile was shown to yield errant results for the particular highly asymmetric configuration, due to the presence of the periodic effects. As such, periodic projectile linear stability analysis must be employed, which uses the machinery of Floquet theory to account for the periodic effects and provide a substantially better estimate of stability boundaries. Key assumptions for the LTP analysis are that the projectile total velocity and roll rate are slowly varying with respect to time and other states. For the case of symmetric projectiles, LTP models reduce to LTI approximations, which yield identical results between Floquet theory and traditional LTI stability predictions.

Funding

This research received no specific grant from any funding agency in the public, commercial, or not-for-profit sectors.

References

1. Morrison PH. A lesson learned about cannon launched guided projectiles. *J Guidance Navigat Control* 1980; 3: 154–157.
2. Morrison PH and Berntson DS. Guidance and control of a cannon-launched guided projectile. *J Spacecraft Rockets* 1977; 14: 328–334.
3. Grubb ND and Belcher MW. Excalibur: new precision engagement asset in the warfight. *Fires* 2008; Oct–Dec: 14–15.
4. Fresconi F. Guidance and control of a projectile with reduced sensor and actuator requirements. *J Guidance Control Dynam* 2011; 34: 1757–1766.
5. Fresconi F and Harkins T. Experimental flight characterization of asymmetric and maneuvering projectiles from elevated gun firings. *J Spacecraft Rockets* 2012; 49: 1120–1130.
6. Cooper G, Costello M and Fresconi F. Flight stability of asymmetric projectiles with control mechanisms. *J Spacecraft Rockets* 2011; 49: 130–135.
7. Fresconi F, Celmins I and Fairfax L. Optimal parameters for maneuverability of affordable precision munitions. In: *2012 AIAA aerospace sciences meeting proceedings*, Orlando, FL, January 12 2012.
8. Fresconi F, Cooper GR, Celmins I, et al. Flight mechanics of a novel guided spin-stabilized projectile concept. *J Aerospace Eng* 2011; 226(3): 327–340.
9. Fowler R, Gallop E, Lock C, et al. *The aerodynamics of the spinning shell*. London: Philosophical Transactions of the Royal Society of London. Series A, 1921, pp.295–387.
10. McCoy RL. *Modern exterior ballistics*. Atgen, PA: Schiffer Military History, 1999.
11. Etkin B. *Dynamics of atmospheric flight*. Dover, DE: Courier Dover Publications, 2012.
12. Szidarovsky F and Bahill AT. *Linear systems theory*. 2nd ed. Boca Raton, FL, USA: CRC Press, 1998.
13. Rogers J and Costello M. Design of a roll-stabilized mortar projectile with reciprocating canards. *J Guidance Control Dynam* 2010; 33: 1026–1034.
14. Murphy CH. Symmetric missile dynamic instabilities: A survey. In: *18th AIAA aerospace sciences meeting*. Pasadena, CA, USA, 14–16 January 1980, paper no. AIAA1980-0320. USA: AIAA.
15. Hodapp AE. Effect of mass asymmetry on ballistic match of projectiles. *J Spacecraft Rockets* 1976; 13: 757–760.
16. Weber DJ. Simplified method for evaluating the flight stability of liquid-filled projectiles. *J Spacecraft Rockets* 1994; 31: 130–134.
17. Murphy CH. Angular motion of a spinning projectile with a viscous liquid payload. *J* Guidance Control Dynam 1983; 6: 280–286.
18. Cobb KK and Whyte RH. Effects of moving components on the motion of a 20-mm projectile. In: *11th AIAA aerodynamics testing conference*. New York: AIAA, 1983, pp. 94–103.
19. Hodapp AE. Passive means for stabilizing projectiles with partially restrained internal members. *J Guidance Control Dynam* 1989; 12: 135–139.
20. Soper WG. Projectile instability produced by internal friction. *AIAA J* 1978; 16: 8–11.
21. Costello M and Peterson A. Linear theory of a dual-spin projectile in atmospheric flight. *J* Guidance Control Dynam 2000; 23: 789–797.
22. Murphy CH. Instability of controlled projectiles in ascending or descending flight. *J Guidance Control* 1981; 4: 66–69.
23. Cooper G. Influence of yaw canards on the yaw growth of spin stabilized projectiles. *J Aircraft* 2001; 38: 266–270.
24. Guidos B and Cooper G. *Closed form solution of finned projectile motion subjected to simple in-flight lateral impulse*. AIAA Paper 2000 0767. New York: AIAA, 2000.
25. Burchett B and Peterson A. Prediction of swerving motion of a dual-spin projectile with lateral pulse jets in atmospheric flight. *Math Comput Model* 2002; 35: 821–834.
26. Ollerenshaw D and Costello M. Model predictive control of a direct fire projectile equipped with canards. *J Dynam Syst Measurement Control* 2008; 35: 114.
27. Cooper G and Fresconi F. Flight stability of an asymmetric projectile with activating canards. In: *AIAA atmospheric flight mechanics conference*, Toronto, CA, May 2010.
28. Montalvo C and Costello M. Effect of canard stall on projectile roll and pitch damping. *J Aerospace Eng* 2011; 225: 1003–1011.

29. Miller R and Michel A. *Ordinary differential equations*. Dover, DE: Dover Publications, 2007.
30. Carlucci D and Jacobson S. *Ballistics: theory and design of guns and ammunition*. Boca Raton, FL, USA: CRC Press, 2007.
31. Murphy CH. Free flight motion of symmetric missiles. Technical Report 1216. MD: Ballistic Research Laboratories, Aberdeen Proving Ground, 1963.
32. Costello M and Anderson D. Effect of internal mass imbalance on the terminal accuracy and stability of a projectile. In: *Proceedings of the 1990 AIAA flight mechanics conference*, San Diego, CA, pp. 29–31. New York: AIAA.
33. Kreyszig E. *Advanced engineering mathematics*. 9th ed. Hoboken, NJ, USA: Wiley, 2006 Chapters 1–3.
34. Brown J and Churchill R. *Complex variables and applications*. 8th ed. Monterey, CA, USA: McGraw-Hill, 2009 Chapter 3.
35. Fresconi F and Brown T. Very affordable precision projectile system and flight experiments. In: *27th Army Science conference*. Orlando, FL, USA, 29 November–2 December 2011.
36. Dupuis A. *Aeroballistic range and wind tunnel tests of the basic finner reference projectile from subsonic to high supersonic velocities*. Technical Report. Canada: Defense Research and Development, 2002.
37. *Prodas version 3 technical manual*. Burlington, VT: Arrow Tech Associates, 2000.

Appendix 1

Notation

$\mathbf{A}$	dynamic matrix of the linearized system
b_{can}	root-to-tip canard length, m
$\boldsymbol{B}$	forcing function vector of the linearized system
c_{can}	canard chord, m
C_{NA}	normal force aerodynamic coefficient
C_{NPA}	Magnus force aerodynamic coefficient
C_{MPA}	Magnus moment aerodynamic coefficient
C_{MQ}	pitch damping moment aerodynamic coefficient
C_{X0}	zero yaw axial force aerodynamic coefficient, parallel to projectile body axis of symmetry
C_{X2}	yaw axial force aerodynamic coefficient, parallel to projectile body axis of symmetry
C_{Y0},C_{Z0}	trim force aerodynamic coefficients, perpendicular to projectile body axis of symmetry
C_{LDD}	roll moment aerodynamic coefficient due to fin cant
C_{LP}	roll damping aerodynamic coefficient
D	projectile reference diameter, m
L, M, N	external moment components on the projectile body expressed in the projectile body reference frame, N-m
m	projectile mass, kg
M	Mach number
p, q, r	angular velocity components of the projectile body expressed in the projectile body reference frame, rad/s
$SLCG$	projectile stationline center of gravity positioning, m
u, v, w	translational velocity components of the projectile mass center expressed in the projectile body reference frame, m/s
V	velocity magnitude of projectile mass center, m
X, Y, Z	total external force components on the projectile body expressed in the projectile body reference frame, N
x, y, z	position vector components of the projectile body mass center expressed in the inertial reference frame, m
α	total aerodynamic angle of attack, °
α_{C_i}	total aerodynamic angle of attack of the ith lifting surface, °
ϕ,θ,ψ	Euler roll, pitch, yaw angles, °

Appendix 2

The extended PLT dynamic matrix $\mathbf{A}$ is populated by the following classical PLT coefficient expressions.

$$C'_{\mathrm{VV}} = -\frac{\pi\rho D^3 C_{\mathrm{X0}}}{8m} \tag{28}$$

$$C'_{\mathrm{pV}} = \frac{\pi\rho D^4 C_{\mathrm{LDD}}}{8I_R} \tag{29}$$

$$C'_{\mathrm{pp}} = \frac{\pi\rho D^5 C_{\mathrm{LP}}}{16I_R} \tag{30}$$

$$C'_{\tilde{v}\tilde{v}} = -\frac{\pi\rho D^3 C_{\mathrm{NA}}}{8m} \tag{31}$$

$$C'_{\tilde{v}\tilde{r}} = -D \tag{32}$$

$$C'_{\tilde{w}\tilde{w}} = -\frac{\pi\rho D^3 C_{\mathrm{NA}}}{8m} \tag{33}$$

$$C'_{\tilde{w}\tilde{q}} = D \tag{34}$$

$$C'_{\tilde{q}\tilde{v}} = -\frac{\pi\rho D^4 C_{\mathrm{YPA}} \Delta \mathrm{SL}_M}{16 I_P V_o} p_o \tag{35}$$

$$C'_{\tilde{q}\tilde{w}} = \frac{\pi\rho D^3 C_{\mathrm{NA}} \Delta \mathrm{SL}}{8I_P} \tag{36}$$

$$C'_{\tilde{q}\tilde{q}} = \frac{\pi\rho D^5 C_{\mathrm{MQ}}}{16I_P} \tag{37}$$

$$C'_{\tilde{q}\tilde{r}} = -\frac{DI_R}{V_o I_P} p_o \tag{38}$$

$$C'_{\tilde{r}\tilde{v}} = -\frac{\pi\rho D^3 C_{\mathrm{NA}} \Delta \mathrm{SL}}{8 I_P} \tag{39}$$

$$C'_{\tilde{r}\tilde{w}} = \frac{\pi\rho D^4 C_{\mathrm{YPA}} \Delta \mathrm{SL}_M}{16 I_P V_o} p_o \tag{40}$$

$$C'_{\tilde{r}\tilde{q}} = \frac{DI_R}{V_o I_P} p_o \tag{41}$$

$$C'_{\tilde{r}\tilde{r}} = \frac{\pi\rho D^5 C_{\mathrm{MQ}}}{16 I_P} \tag{42}$$

$$G'_V = \frac{Dg\sin[\theta_o]}{V_o} \tag{43}$$

$$G'_{\tilde{w}} = \frac{Dg\cos[\theta_o]}{V_o} \tag{44}$$

The extended PLT dynamic matrix **A** is populated by the following extended PLT coefficient expressions.

$$X'_V = -\frac{\pi\rho D^3 C_{D_o}}{8m} n \tag{45}$$

$$X'_p = \frac{\pi\rho D^3 C_{L_\alpha}}{8m} \sum_{i=1}^{n} \delta_{C_i} (\cos[\phi_{C_i}] \Delta \mathrm{BL}_{C_i} + \sin[\phi_{C_i}] \Delta \mathrm{WL}_{C_i}) \tag{46}$$

$$X'_{\mathrm{pp}} = \frac{\pi\rho D^3 C_{L_\alpha}}{8mV} \sum_{i=1}^{n} (\cos[\phi_{C_i}] \Delta \mathrm{BL}_{C_i} + \sin[\phi_{C_i}] \Delta \mathrm{WL}_{C_i})^2 \tag{47}$$

$$X'_{\tilde{v}} = -\frac{\pi\rho D^3 C_{L_\alpha}}{8m} \sum_{i=1}^{n} \sin[\phi + \phi_{C_i}] \delta_{C_i} \tag{48}$$

$$X'_{\tilde{v}p} = -\frac{\pi\rho D^3 C_{L_\alpha}}{4mV} \sum_{i=1}^{n} \sin[\phi + \phi_{C_i}] \cdot (\cos[\phi_{C_i}] \Delta \mathrm{BL}_{C_i} + \sin[\phi_{C_i}] \Delta \mathrm{WL}_{C_i}) \tag{49}$$

$$X'_{\tilde{w}} = \frac{\pi\rho D^3 C_{L_\alpha}}{8m} \sum_{i=1}^{n} \cos[\phi + \phi_{C_i}] \delta_{C_i} \tag{50}$$

$$X'_{\tilde{w}p} = \frac{\pi\rho D^3 C_{L_\alpha}}{4mV} \sum_{i=1}^{n} \cos[\phi + \phi_{C_i}] \cdot (\cos[\phi_{C_i}] \Delta \mathrm{BL}_{C_i} + \sin[\phi_{C_i}] \Delta \mathrm{WL}_{C_i}) \tag{51}$$

$$X'_{\tilde{q}} = -\frac{\pi\rho D^3}{8m} \sum_{i=1}^{n} (\cos[\phi + \phi_{C_i}] C_{L_\alpha} \delta_{C_i} \Delta \mathrm{SL}_{C_i} + C_{D_o} \cdot (\sin[\phi] \Delta \mathrm{BL}_{C_i} + \cos[\phi] \Delta \mathrm{WL}_{C_i})) \tag{52}$$

$$X'_{\tilde{q}p} = -\frac{\pi\rho D^3}{4mV} \sum_{i=1}^{n} \cos[\phi + \phi_{C_i}] C_{L_\alpha} \Delta \mathrm{SL}_{C_i} \cdot (\cos[\phi_{C_i}] \Delta \mathrm{BL}_{C_i} + \sin[\phi_{C_i}] \Delta \mathrm{WL}_{C_i}) \tag{53}$$

$$X'_{\tilde{r}} = -\frac{\pi\rho D^3}{8m} \sum_{i=1}^{n} (\sin[\phi + \phi_{C_i}] \delta_{C_i} C_{L_\alpha} \Delta \mathrm{SL}_{C_i} - C_{D_o} \cdot (\cos[\phi] \Delta \mathrm{BL}_{C_i} - \sin[\phi] \Delta \mathrm{WL}_{C_i})) \tag{54}$$

$$X'_{\tilde{r}p} = -\frac{\pi\rho D^3 C_{L_\alpha}}{4mV} \sum_{i=1}^{n} \sin[\phi + \phi_{C_i}] \Delta \mathrm{SL}_{C_i} \cdot (\cos[\phi_{C_i}] \Delta \mathrm{BL}_{C_i} + \sin[\phi_{C_i}] \Delta \mathrm{WL}_{C_i}) \tag{55}$$

$$Y'_V = \frac{\pi\rho D^3 C_{L_\alpha}}{8m} \sum_{i=1}^{n} \sin[\phi + \phi_{C_i}] \delta_{C_i} \tag{56}$$

$$Y'_p = \frac{\pi\rho D^3 (C_{D_o} + C_{L_\alpha})}{8m} \sum_{i=1}^{n} \sin[\phi + \phi_{C_i}] \cdot (\cos[\phi_{C_i}] \Delta \mathrm{BL}_{C_i} + \sin[\phi_{C_i}] \Delta \mathrm{WL}_{C_i}) \tag{57}$$

$$Y'_{\mathrm{pp}} = 0 \tag{58}$$

$$Y'_{\tilde{v}} = -\frac{\pi\rho D^3 (C_{D_o} + C_{L_\alpha})}{8m} \sum_{i=1}^{n} \sin[\phi + \phi_{C_i}]^2 \tag{59}$$

$$Y'_{\tilde{v}p} = 0 \tag{60}$$

$$Y'_{\tilde{w}} = \frac{\pi\rho D^3 (C_{D_o} + C_{L_\alpha})}{16m} \sum_{i=1}^{n} \sin[2(\phi + \phi_{C_i})] \tag{61}$$

$$Y'_{\tilde{w}p} = 0 \tag{62}$$

$$Y'_{\tilde{q}} = -\frac{\pi\rho D^3}{8m} \sum_{i=1}^{n} \sin[\phi + \phi_{C_i}] \cdot ((C_{D_o} + C_{L_\alpha}) \cos[\phi + \phi_{C_i}] \Delta \mathrm{SL}_{C_i} - C_{L_\alpha} \delta_{C_i} (\sin[\phi] \Delta \mathrm{BL}_{C_i} + \cos[\phi] \Delta \mathrm{WL}_{C_i})) \tag{63}$$

$$Y'_{\tilde{q}p} = \frac{\pi\rho D^3 C_{L_\alpha}}{8mV} \sum_{i=1}^{n} \sin[\phi + \phi_{C_i}] \cdot (\sin[\phi] \Delta \mathrm{BL}_{C_i} + \cos[\phi] \Delta \mathrm{WL}_{C_i}) \cdot (\cos[\phi_{C_i}] \Delta \mathrm{BL}_{C_i} + \sin[\phi_{C_i}] \Delta \mathrm{WL}_{C_i}) \tag{64}$$

$$Y'_{\tilde{r}} = -\frac{\pi\rho D^3}{8m} \sum_{i=1}^{n} \sin[\phi + \phi_{C_i}] \cdot ((C_{D_o} + C_{L_\alpha}) \sin[\phi + \phi_{C_i}] \Delta \mathrm{SL}_{C_i} + C_{L_\alpha} \delta_{C_i} (\cos[\phi] \Delta \mathrm{BL}_{C_i} - \sin[\phi] \Delta \mathrm{WL}_{C_i})) \tag{65}$$

$$Y'_{\tilde{r}p} = -\frac{\pi\rho D^3 C_{L_\alpha}}{8mV}\sum_{i=1}^{n}\sin[\phi+\phi_{C_i}] \cdot(\cos[\phi]\Delta\mathrm{BL}_{C_i}-\sin[\phi]\Delta\mathrm{WL}_{C_i}) \cdot(\cos[\phi_{C_i}]\Delta\mathrm{BL}_{C_i}+\sin[\phi_{C_i}]\Delta\mathrm{WL}_{C_i}) \quad (66)$$

$$Z'_V = -\frac{\pi\rho D^3}{8m}\sum_{i=1}^{n}\cos[\phi+\phi_{C_i}]C_{L_\alpha}\delta_{C_i} \quad (67)$$

$$Z'_p = -\frac{\pi\rho D^3(C_{D_o}+C_{L_\alpha})}{8m}\sum_{i=1}^{n}\cos[\phi+\phi_{C_i}] \cdot(\cos[\phi_{C_i}]\Delta\mathrm{BL}_{C_i}+\sin[\phi_{C_i}]\Delta\mathrm{WL}_{C_i}) \quad (68)$$

$$Z'_{\mathrm{pp}} = 0 \quad (69)$$

$$Z'_{\tilde{v}} = \frac{\pi\rho D^3(C_{D_o}+C_{L_\alpha})}{16m}\sum_{i=1}^{n}\sin[2(\phi+\phi_{C_i})] \quad (70)$$

$$Z'_{\tilde{v}p} = 0 \quad (71)$$

$$Z'_{\tilde{w}} = -\frac{\pi\rho D^3(C_{D_o}+C_{L_\alpha})}{8m}\sum_{i=1}^{n}\cos[\phi+\phi_{C_i}]^2 \quad (72)$$

$$Z'_{\tilde{w}p} = 0 \quad (73)$$

$$Z'_{\tilde{q}} = \frac{\pi\rho D^3}{8m}\sum_{i=1}^{n}\cos[\phi+\phi_{C_i}]((C_{D_o}+C_{L_\alpha}) \cdot\cos[\phi+\phi_{C_i}]\Delta\mathrm{SL}_{C_i} - C_{L_\alpha}\delta_{C_i}(\sin[\phi]\Delta\mathrm{BL}_{C_i}+\cos[\phi]\Delta\mathrm{WL}_{C_i})) \quad (74)$$

$$Z'_{\tilde{q}p} = -\frac{\pi\rho D^3 C_{L_\alpha}}{8mV}\sum_{i=1}^{n}\cos[\phi+\phi_{C_i}] \cdot(\sin[\phi]\Delta\mathrm{BL}_{C_i}+\cos[\phi]\Delta\mathrm{WL}_{C_i}) \cdot(\cos[\phi_{C_i}]\Delta\mathrm{BL}_{C_i}+\sin[\phi_{C_i}]\Delta\mathrm{WL}_{C_i}) \quad (75)$$

$$Z'_{\tilde{r}} = \frac{\pi\rho D^3}{8m}\sum_{i=1}^{n}\cos[\phi+\phi_{C_i}]((C_{D_o}+C_{L_\alpha}) \cdot\sin[\phi+\phi_{C_i}]\Delta\mathrm{SL}_{C_i} + C_{L_\alpha}\delta_{C_i}(\cos[\phi]\Delta\mathrm{BL}_{C_i}-\sin[\phi]\Delta\mathrm{WL}_{C_i})) \quad (76)$$

$$Z'_{\tilde{r}p} = \frac{\pi\rho D^3 C_{L_\alpha}}{8mV}\sum_{i=1}^{n}\cos[\phi+\phi_{C_i}] \cdot(\cos[\phi]\Delta\mathrm{BL}_{C_i}-\sin[\phi]\Delta\mathrm{WL}_{C_i}) \cdot(\cos[\phi_{C_i}]\Delta\mathrm{BL}_{C_i}+\sin[\phi_{C_i}]\Delta\mathrm{WL}_{C_i}) \quad (77)$$

$$L'_p = -\frac{\pi\rho D^3(C_{D_o}+C_{L_\alpha})}{8I_R}\sum_{i=1}^{n}(\cos[\phi_{C_i}]\Delta\mathrm{BL}_{C_i} +\sin[\phi_{C_i}]\Delta\mathrm{WL}_{C_i})^2 \quad (78)$$

$$L'_{\mathrm{pp}} = 0 \quad (79)$$

$$L'_{\tilde{v}} = \frac{\pi\rho D^3(C_{D_o}+C_{L_\alpha})}{8I_R}\sum_{i=1}^{n}\sin[\phi+\phi_{C_i}] \cdot(\cos[\phi_{C_i}]\Delta\mathrm{BL}_{C_i}+\sin[\phi_{C_i}]\Delta\mathrm{WL}_{C_i}) \quad (80)$$

$$L'_{\tilde{v}p} = 0 \quad (81)$$

$$L'_{\tilde{w}} = -\frac{\pi\rho D^3(C_{D_o}+C_{L_\alpha})}{8I_R}\sum_{i=1}^{n}\cos[\phi+\phi_{C_i}] \cdot(\cos[\phi_{C_i}]\Delta\mathrm{BL}_{C_i}+\sin[\phi_{C_i}]\Delta\mathrm{WL}_{C_i}) \quad (82)$$

$$L'_{\tilde{w}p} = 0 \quad (83)$$

$$L'_{\tilde{q}} = \frac{\pi\rho D^3}{8I_R}\sum_{i=1}^{n}(\cos[\phi_{C_i}]\Delta\mathrm{BL}_{C_i}+\sin[\phi_{C_i}]\Delta\mathrm{WL}_{C_i}) \cdot((C_{D_o}+C_{L_\alpha})\cos[\phi+\phi_{C_i}]\Delta\mathrm{SL}_{C_i} - C_{L_\alpha}\delta_{C_i}(\sin[\phi]\Delta\mathrm{BL}_{C_i}+\cos[\phi]\Delta\mathrm{WL}_{C_i})) \quad (84)$$

$$L'_{\tilde{q}p} = -\frac{\pi\rho D^3 C_{L_\alpha}}{8I_R V}\sum_{i=1}^{n}(\sin[\phi]\Delta\mathrm{BL}_{C_i}+\cos[\phi]\Delta\mathrm{WL}_{C_i}) \cdot(\cos[\phi_{C_i}]\Delta\mathrm{BL}_{C_i}+\sin[\phi_{C_i}]\Delta\mathrm{WL}_{C_i})^2 \quad (85)$$

$$L'_{\tilde{r}} = \frac{\pi\rho D^3}{8I_R}\sum_{i=1}^{n}(\cos[\phi_{C_i}]\Delta\mathrm{BL}_{C_i}+\sin[\phi_{C_i}]\Delta\mathrm{WL}_{C_i}) \cdot((C_{D_o}+C_{L_\alpha})\sin[\phi+\phi_{C_i}]\Delta\mathrm{SL}_{C_i} + C_{L_\alpha}\delta_{C_i}(\cos[\phi]\Delta\mathrm{BL}_{C_i}-\sin[\phi]\Delta\mathrm{WL}_{C_i})) \quad (86)$$

$$L'_{\tilde{r}p} = \frac{\pi\rho D^3 C_{L_\alpha}}{8I_R V}\sum_{i=1}^{n}(\cos[\phi]\Delta\mathrm{BL}_{C_i}-\sin[\phi]\Delta\mathrm{WL}_{C_i}) \cdot(\cos[\phi_{C_i}]\Delta\mathrm{BL}_{C_i}+\sin[\phi_{C_i}]\Delta\mathrm{WL}_{C_i})^2 \quad (87)$$

$$M'_V = -\frac{\pi\rho D^3}{8I_P}\sum_{i=1}^{n}(-\cos[\phi+\phi_{C_i}]C_{L_\alpha}\delta_{C_i}\Delta\mathrm{SL}_{C_i}+C_{D_o} \cdot(\sin[\phi]\Delta\mathrm{BL}_{C_i}+\cos[\phi]\Delta\mathrm{WL}_{C_i})) \quad (88)$$

$$M'_p = \frac{\pi\rho D^3}{8I_P}\sum_{i=1}^{n}(\cos[\phi_{C_i}]\Delta\mathrm{BL}_{C_i}+\sin[\phi_{C_i}]\Delta\mathrm{WL}_{C_i}) \cdot((C_{D_o}+C_{L_\alpha})\cos[\phi+\phi_{C_i}]\Delta\mathrm{SL}_{C_i} + C_{L_\alpha}\delta_{C_i}(\sin[\phi]\Delta\mathrm{BL}_{C_i}+\cos[\phi]\Delta\mathrm{WL}_{C_i})) \quad (89)$$

$$M'_{\mathrm{pp}} = \frac{\pi\rho D^3 C_{L_\alpha}}{8I_P V}\sum_{i=1}^{n}(\sin[\phi]\Delta\mathrm{BL}_{C_i}+\cos[\phi]\Delta\mathrm{WL}_{C_i}) \cdot(\cos[\phi_{C_i}]\Delta\mathrm{BL}_{C_i}+\sin[\phi_{C_i}]\Delta\mathrm{WL}_{C_i})^2 \quad (90)$$

$$M'_{\tilde{v}} = -\frac{\pi\rho D^3}{8I_P}\sum_{i=1}^{n}\sin[\phi+\phi_{C_i}]((C_{D_o}+C_{L_\alpha}) \cdot\cos[\phi+\phi_{C_i}]\Delta\mathrm{SL}_{C_i} + C_{L_\alpha}\delta_{C_i}(\sin[\phi]\Delta\mathrm{BL}_{C_i}+\cos[\phi]\Delta\mathrm{WL}_{C_i})) \quad (91)$$

$$M'_{\tilde{v}p} = -\frac{\pi\rho D^3 C_{L_\alpha}}{4I_P V}\sum_{i=1}^{n}\sin[\phi+\phi_{C_i}] \cdot(\sin[\phi]\Delta\mathrm{BL}_{C_i}+\cos[\phi]\Delta\mathrm{WL}_{C_i}) \cdot(\cos[\phi_{C_i}]\Delta\mathrm{BL}_{C_i}+\sin[\phi_{C_i}]\Delta\mathrm{WL}_{C_i}) \quad (92)$$

$$M'_{\tilde{w}} = \frac{\pi\rho D^3}{8I_P}\sum_{i=1}^{n}\cos[\phi+\phi_{C_i}] \cdot((C_{D_o}+C_{L_\alpha})\cos[\phi+\phi_{C_i}]\Delta\mathrm{SL}_{C_i} + C_{L_\alpha}\delta_{C_i}(\sin[\phi]\Delta\mathrm{BL}_{C_i}+\cos[\phi]\Delta\mathrm{WL}_{C_i})) \quad (93)$$

$$M'_{\tilde{w}p} = \frac{\pi\rho D^3 C_{L_\alpha}}{4I_P V}\sum_{i=1}^{n}\cos[\phi+\phi_{C_i}] \cdot(\sin[\phi]\Delta\mathrm{BL}_{C_i}+\cos[\phi]\Delta\mathrm{WL}_{C_i}) \cdot(\cos[\phi_{C_i}]\Delta\mathrm{BL}_{C_i}+\sin[\phi_{C_i}]\Delta\mathrm{WL}_{C_i}) \quad (94)$$

$$M'_{\tilde{q}} = -\frac{\pi\rho D^3}{8I_P}\sum_{i=1}^{n}((C_{D_o}+C_{L_\alpha})\cos[\phi+\phi_{C_i}]^2\Delta\mathrm{SL}_{C_i}^2 + C_{D_o}(\sin[\phi]\Delta\mathrm{BL}_{C_i}+\cos[\phi]\Delta\mathrm{WL}_{C_i})^2) \quad (95)$$

$$M'_{\tilde{q}p} = -\frac{\pi\rho D^3 C_{L_\alpha}}{8I_P V}\sum_{i=1}^{n}\cos[\phi+\phi_{C_i}]\Delta\mathrm{SL}_{C_i} \cdot(\sin[\phi]\Delta\mathrm{BL}_{C_i}+\cos[\phi]\Delta\mathrm{WL}_{C_i}) \cdot(\cos[\phi_{C_i}]\Delta\mathrm{BL}_{C_i}+\sin[\phi_{C_i}]\Delta\mathrm{WL}_{C_i}) \quad (96)$$

$$M'_{\tilde{r}} = -\frac{\pi\rho D^3}{16I_P}\sum_{i=1}^{n}(C_{L_\alpha}\Delta\mathrm{SL}_{C_i}(\sin[2(\phi+\phi_{C_i})] \Delta\mathrm{SL}_{C_i}+2\delta_{C_i}\times(\cos[\phi_{C_i}]\Delta\mathrm{BL}_{C_i}+\sin[\phi_{C_i}] \Delta\mathrm{WL}_{C_i}))+C_{D_o}(\sin[2(\phi+\phi_{C_i})] \cdot\Delta\mathrm{SL}_{C_i}^2-2\cos[2\phi]\Delta\mathrm{BL}_{C_i}\Delta\mathrm{WL}_{C_i} \cdot+\sin[2\phi](-\Delta\mathrm{BL}_{C_i}^2+\Delta\mathrm{WL}_{C_i}^2))) \quad (97)$$

$$M'_{\tilde{r}p} = -\frac{\pi\rho D^3 C_{L_\alpha}}{16I_P V}\sum_{i=1}^{n}\Delta\mathrm{SL}_{C_i} \cdot(-\cos[\phi_{C_i}](-3\cos[\phi_{C_i}]+\cos[2\phi+\phi_{C_i}]) \cdot\Delta\mathrm{BL}_{C_i}^2+(\sin[2\phi]+3\sin[2\phi_{C_i}])\Delta\mathrm{BL}_{C_i} \cdot\Delta\mathrm{WL}_{C_i}\times+\sin[\phi_{C_i}](3\sin[\phi_{C_i}] +\sin[2\phi+\phi_{C_i}])\Delta\mathrm{WL}_{C_i}^2) \quad (98)$$

$$N'_V = \frac{\pi\rho D^3}{8I_P}\sum_{i=1}^{n}(\sin[\phi+\phi_{C_i}]C_{L_\alpha}\delta_{C_i}\Delta\mathrm{SL}_{C_i}+C_{D_o} \cdot(\cos[\phi]\Delta\mathrm{BL}_{C_i}-\sin[\phi]\Delta\mathrm{WL}_{C_i})) \quad (99)$$

$$N'_p = \frac{\pi\rho D^3}{8I_P}\sum_{i=1}^{n}(\cos[\phi_{C_i}]\Delta\mathrm{BL}_{C_i}+\sin[\phi_{C_i}]\Delta\mathrm{WL}_{C_i}) \cdot((C_{D_o}+C_{L_\alpha})\sin[\phi+\phi_{C_i}]\Delta\mathrm{SL}_{C_i} - C_{L_\alpha}\delta_{C_i}(\cos[\phi]\Delta\mathrm{BL}_{C_i}-\sin[\phi]\Delta\mathrm{WL}_{C_i})) \quad (100)$$

$$N'_{\mathrm{pp}} = -\frac{\pi\rho D^3 C_{L_\alpha}}{8I_P V}\sum_{i=1}^{n}(\cos[\phi]\Delta\mathrm{BL}_{C_i}-\sin[\phi]\Delta\mathrm{WL}_{C_i}) \cdot(\cos[\phi_{C_i}]\Delta\mathrm{BL}_{C_i}+\sin[\phi_{C_i}]\Delta\mathrm{WL}_{C_i})^2 \quad (101)$$

$$N'_{\tilde{v}} = -\frac{\pi\rho D^3}{8I_P}\sum_{i=1}^{n}\sin[\phi+\phi_{C_i}]((C_{D_o}+C_{L_\alpha}) \cdot\sin[\phi+\phi_{C_i}]\Delta\mathrm{SL}_{C_i} - C_{L_\alpha}\delta_{C_i}(\cos[\phi]\Delta\mathrm{BL}_{C_i}-\sin[\phi]\Delta\mathrm{WL}_{C_i})) \quad (102)$$

$$N'_{\tilde{v}p} = \frac{\pi\rho D^3 C_{L_\alpha}}{4I_P V}\sum_{i=1}^{n}\sin[\phi+\phi_{C_i}] \cdot(\cos[\phi]\Delta\mathrm{BL}_{C_i}-\sin[\phi]\Delta\mathrm{WL}_{C_i}) \cdot(\cos[\phi_{C_i}]\Delta\mathrm{BL}_{C_i}+\sin[\phi_{C_i}]\Delta\mathrm{WL}_{C_i}) \quad (103)$$

$$N'_{\tilde{w}} = \frac{\pi\rho D^3}{8I_P}\sum_{i=1}^{n}\cos[\phi+\phi_{C_i}]((C_{D_o}+C_{L_\alpha}) \cdot\sin[\phi+\phi_{C_i}]\Delta\mathrm{SL}_{C_i} - C_{L_\alpha}\delta_{C_i}(\cos[\phi]\Delta\mathrm{BL}_{C_i}-\sin[\phi]\Delta\mathrm{WL}_{C_i})) \quad (104)$$

$$N'_{\tilde{w}p} = -\frac{\pi\rho D^3 C_{L_\alpha}}{4I_P V}\sum_{i=1}^{n}\cos[\phi+\phi_{C_i}] \cdot(\cos[\phi]\Delta\mathrm{BL}_{C_i}-\sin[\phi]\Delta\mathrm{WL}_{C_i}) \cdot(\cos[\phi_{C_i}]\Delta\mathrm{BL}_{C_i}+\sin[\phi_{C_i}]\Delta\mathrm{WL}_{C_i}) \quad (105)$$

$$N'_{\tilde{q}} = \frac{D^3\pi\rho}{16I_P}\sum_{i=1}^{n}(C_{L_\alpha}\Delta\mathrm{SL}_{C_i}(-\sin[2(\phi+\phi_{C_i})]\Delta\mathrm{SL}_{C_i} +2\delta_{C_i}(\cos[\phi_{C_i}]\Delta\mathrm{BL}_{C_i}+\sin[\phi_{C_i}]\Delta\mathrm{WL}_{C_i})) +C_{D_o}(-\sin[2(\phi+\phi_{C_i})]\Delta\mathrm{SL}_{C_i}^2+2\cos[2\phi] \cdot\Delta\mathrm{BL}_{C_i}\Delta\mathrm{WL}_{C_i}+\sin[2\phi](\Delta\mathrm{BL}_{C_i}^2-\Delta\mathrm{WL}_{C_i}^2))) \quad (106)$$

$$N'_{\tilde{q}p} = \frac{\pi\rho D^3 C_{L_\alpha}}{16I_P V}\sum_{i=1}^{n}\Delta\mathrm{SL}_{C_i} \cdot(\cos[\phi_{C_i}](3\cos[\phi_{C_i}]+\cos[2\phi+\phi_{C_i}])\Delta\mathrm{BL}_{C_i}^2 -(\sin[2\phi]-3\sin[2\phi_{C_i}])\Delta\mathrm{BL}_{C_i}\Delta\mathrm{WL}_{C_i} -\sin[\phi_{C_i}](-3\sin[\phi_{C_i}]+\sin[2\phi+\phi_{C_i}])\Delta\mathrm{WL}_{C_i}^2) \quad (107)$$

$$N'_{\tilde{r}} = -\frac{\pi\rho D^3}{8I_P}\sum_{i=1}^{n}((C_{D_o}+C_{L_\alpha})\sin[\phi+\phi_{C_i}]^2\Delta\mathrm{SL}_{C_i}^2 + C_{D_o}(\cos[\phi]\Delta\mathrm{BL}_{C_i}-\sin[\phi]\Delta\mathrm{WL}_{C_i})^2) \quad (108)$$

$$N'_{\tilde{r}p} = \frac{\pi\rho D^3 C_{L_\alpha}}{8I_P V}\sum_{i=1}^{n}\sin[\phi+\phi_{C_i}]\Delta\mathrm{SL}_{C_i} \cdot(\cos[\phi]\Delta\mathrm{BL}_{C_i}-\sin[\phi]\Delta\mathrm{WL}_{C_i}) \cdot(\cos[\phi_{C_i}]\Delta\mathrm{BL}_{C_i}+\sin[\phi_{C_i}]\Delta\mathrm{WL}_{C_i}) \quad (109)$$